

Influenza Viral Membrane Deformation due to Refolding of HA-protein: Two-dimensional Model and Analysis

Naveen K. Vaidya^{1,2} and Huaxiong Huang^{2,*}

¹ *Theoretical Biology and Biophysics Group, MS K710, Los Alamos National Laboratory, Los Alamos, NM 87545 USA*

² *Department of Mathematics and Statistics, York University, Toronto, M3J 1P3 Canada*

Abstract. In this paper we study influenza viral membrane deformation related to the refolding of Hemagglutinin (HA) protein. The focus of the paper is to understand membrane deformation and budding due to experimentally observed linear HA-protein clusters, which have not been mathematically studied before. The viral membrane is modeled as a two dimensional incompressible lipid bilayer with bending rigidity. For tensionless membranes, we derive an analytical solution while for membrane under tension we solve the problem numerically. Our solution for tensionless membranes shows that the height of membrane deformation increases monotonically with the bending moment exerted by HA-proteins and attains its maximum when the size of the protein cluster reaches a critical value. Our results also show that the hypothesis of dimple formation proposed in the literature is valid in the two dimensional setting. Our comparative study of axisymmetric HA-clusters and linear HA-clusters reveals that the linear HA-clusters are not favorable to provide a sufficient energy required to overcome an energy barrier for a successful fusion, despite their capability to cause membrane deformation and budding.

Key words: Hemagglutinin Protein; Influenza Virus; Membrane Deformation, Membrane Fusion.

1 Introduction

An influenza virus first attaches to a host cell surface via a sialic acid binding site and then enters the cell by endocytosis process. In the cytoplasm of the cell, when pH-value is lowered, hemagglutinin (HA) protein anchored in the viral membrane

*Corresponding author.

Email: nvaidya@lanl.gov (N.K. Vaidya), hhuang@yorku.ca (H. Huang)

undergoes a conformational change [7, 11, 13]. HA is a trimer of three monomers anchored in the membrane, connected to each other forming a triple-stranded α -helical coiled-coil. During conformational change, recruitment of additional residues to the coiled-coil as well as tilting of the HA-molecule take place [2, 6, 7, 18, 32, 35]. This process exerts force on the membrane. As a result, the membrane deforms leading to a budding to mediate efficient virus-cell fusion.

A study of pre-fusion membrane deformation and budding is important in order to understand the fusion of two membranes, which is the key stage for virus infection and replication. Understanding the role of HA-protein in deforming membrane is useful for various purposes such as disease control and drug/vaccine design. Recently, an antibody has been identified, which can recognize a highly conserved helical region in the membrane-proximal stem of HA1/HA2 [10, 30]. This antibody is found to be capable of neutralizing the viruses behind bird flu and the 1918-19 flu pandemic along with some of the common strains that cause seasonal flu, by blocking conformational rearrangements associated with membrane fusion. Since the helix identified by that antibody and fusion peptides of HA, which enter the target cell membrane are highly conserved among influenza viruses of different strains, vaccines or/and drugs targeting these regions of HA causing fusion inhibition are more efficient to disable multiple varieties of the flu virus [10, 30], which becomes more important during influenza pandemic. It is thus becoming more essential to understand membrane deformation and budding mechanism governed by HA-protein.

Even though the deformation of membrane due to HA-protein is very important, few attempts have been made to quantitatively study this process. In [18], it was hypothesized that the activated HA-protein can produce viral membrane dimples surrounded by a ring-like cluster of HA. They have assumed that the top of the dimple is a segment of perfect sphere connected to a funnel of a catenoid form (an axisymmetric surface with zero mean curvature). Similarly, in [19], HA has been assumed to produce a perfectly spherical top of the dimple. In [25], the formation of a dimple was also favored as a mechanism for membranes to make intimate contact which leads to subsequent fusion between membranes. For an axisymmetric membrane, we have computed numerically the formation of the dimple caused by a ring-like HA-protein cluster [36].

In reality, the distribution of HA-proteins depends on membrane compositions, and especially a quite distinct distribution has been observed between lipid rafts (microdomains enriched in sphingomyelin and cholesterol) and nonraft regions of the membrane [16, 20, 31]. It was found experimentally in [16, 20, 31] that they typically form clusters in the raft-associated membrane sections while nonraft HA distributed mostly randomly at the plasma membrane. It has been estimated that as much as $\sim 50\%$ of the cellular membrane exists as lipid rafts [20]. Furthermore, experimental evidence shows that influenza virus buds from rafts while nonraft HA contains reduced amount of infectivity because HA clusters in rafts provide a sufficient concentration of HA in budding virus required for virus-cell fusion [20, 31]. Therefore, as far as the membrane deformation and the budding related to the fusion is concerned,

HA-proteins have to be considered in clusters. This is also supported by an experiment [9] which showed HA-mediated fusion requires a concerted and cooperative action of at least three to four HA trimers.

A ring-like HA-protein cluster produces quite satisfactory membrane deformation and budding required for fusion activity [18, 36]. However, a quantitative electron microscopy and fluorescence spectroscopy experiment of the membrane distribution of influenza HA have revealed that ring-like clusters are observed only occasionally while majority of the HA-protein clusters bear many other shapes [16]. Moreover, a change in the concentration of sphingomyelin and cholesterol in lipid raft regions also alters the pattern of clustering, especially at the shortest lengths. In [16], clusters are also found in many length scales. A linear dimensional analysis of plasma membrane by using thin sections of wild-type virus has shown enough activities of virus budding [31]. This demands a study of membrane deformation and budding due to HA-protein clusters of the linear structure.

In this paper, we examine the role of linear HA-protein clusters on membrane deformation and budding, which have not been mathematically studied before. Experimental results of HA-protein clustering in two-dimensional membrane (linear dimensional analysis of plasma membrane by using thin section of 363 gold particles labeling wild-type trimeric HA) [31] are consistent with the experimental results in three-dimensional membrane (analysis of 8245 gold particles labeling trimeric HA in membrane surface) [16]. Moreover, enough number of virus budding was observed from the thin section of membrane considered in [31]. This shows that the two-dimensional membrane can reasonably approximate many important properties relevant to the budding and fusion. Moreover, the two-dimensional membrane makes the problems extremely simple and amenable to mathematical analysis. Therefore, we utilize a two-dimensional model of the viral membrane in the form of an energy functional, which incorporates energies due to the bending rigidity of the membrane and the refolding of HA-proteins. Not only did our two-dimensional approach allow us to obtain analytical solution, but it also provided some new results regarding membrane tension, asymmetric protein force and comparison between linear and axisymmetric protein clusters.

In section 2 we present our mathematical model. We carry out analysis of the model in section 3 and derive explicit formulas for the tension and the bending moment developed in the membrane. We also derive the equilibrium shape equation of the membrane by applying force and torque balance and an analytical solution for tensionless membranes. In section 4, we present the results for tensionless membrane and membrane with tension. Our analytical solution for tensionless membrane reveals that the deformed membrane consists of a patch of circular arcs. Based on the analytical expression for the membrane height, we derive the condition for optimal protein cluster size of membrane deformation. Our results confirm the dimple formation of the membrane due to HA-protein, with or without prior membrane tension, in the two dimensional setting. Parametric studies are also carried out, including the effect on membrane shape due to asymmetric bending moments. We also carry out

a comparative study between linear HA-clusters and axisymmetric HA-clusters, and find that linear HA-clusters are not favorable for a successful fusion, despite its capability to cause membrane deformation and budding. We finish the paper with a short conclusion in section 5.

2 Model

Since hemagglutinin (HA) protein anchored on influenza virus membrane is responsible and independently capable for membrane bending required for fusion activity [29], we consider only HA protein in our model while neglecting neuraminidase (another protein) in the viral membrane. HA is a glycoprotein which consists of a trimer with an individual monomer having HA1 and HA2 subunits [3, 13, 18, 21, 24, 32–34]. It is believed that HA1 is responsible for virus attachment to the cell surface via a sialic acid binding site and HA2 activates the fusion process. During low-pH activation (e.g., when the protein is exposed to a pH 5 environment) the hydrophobic fusion peptide, previously hidden within the trimeric stem, is projected towards viral and/or target membranes [3, 11, 18, 28]. The subsequent refolding (which includes tilting as well) of the protein exerts a force on the viral membrane.

We consider a lipid raft region of the membrane as the membrane budding and infectivity mainly occur in the raft regions [20, 31]. We further consider HA-protein in the form of clusters as in [18, 36] because the clustering of HA in lipid raft regions is an intrinsic property of HA-protein and the membrane deformation and budding required for fusion activity is due to a concerted and cooperative action of HA trimers in the cluster [9, 16, 20, 31]. In [18, 36], it was assumed that these HA-protein clusters form ring-like structures and subsequently axis-symmetry was assumed as an approximation. On the other hand, experimental evidence shows that these clusters are formed in many different structures and sizes [16]. Since the HA-protein clusters of linear structure in a linear dimensional analysis of plasma membrane by using thin sections of wild-type virus has been found to be effective to bring virus budding [31], we consider HA-protein clusters of linear structure in this study. Moreover, a consistency between HA-clustering experimental results in two-dimensional (thin section) and three-dimensional membranes validates the two-dimensional membrane model to reasonably approximate many properties relevant to membrane deformation and budding required for fusion [16, 31]. Therefore, here we present a model for two-dimensional membrane deformation caused by HA-protein clusters with a linear formation. We note that to thoroughly study the geometric effect of different cluster formations, one must use a three-dimensional model.

As in [18] and [36], we represent the net effect of the force due to the refolding of HA-trimers in a cluster by a bending moment acting on the membrane. We consider a small section of the two dimensional viral membrane containing a HA-protein cluster as shown in the schematic representation in Fig. 1(a). ds is the arc length of undeformed (neutral pH) membrane measured along the mid-surface. The protein

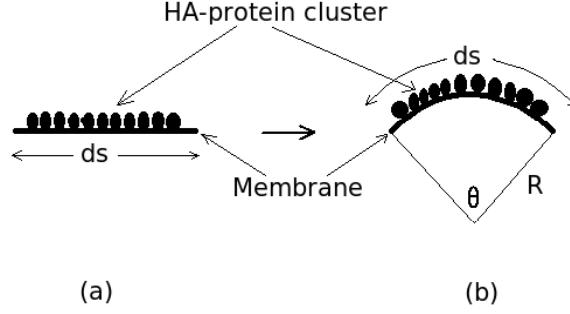


Figure 1: (a) Schematic diagram of the two dimensional undeformed viral membrane segment ds containing a HA-protein cluster. (b) Deformed viral membrane segment ds with curvature R^{-1} and the related angle θ .

molecule in a cluster contains three monomers anchored in the membrane, connected to each other forming a triple-stranded α -helical coiled-coil. When the pH value is lowered, recruitment of additional residues to the coiled-coil takes place [6,7,18]. This results in an extension of the coiled-coils rigid rod, which causes the HA-protein cluster to exert forces (bending moments) on the membrane and the membrane deforms, as shown in Fig. 1(b).

Let c be the curvature of the deformed membrane, c.f. Fig. 1(b). Let m_p be the bending moment per unit length exerted by HA-protein cluster at the ends of the membrane segment. To produce a curvature c of the membrane segment, the work performed by the bending moment is $m_p\theta/2$, where θ is the angle subtended by the circular curved membrane at the center of the circle and R is the corresponding radius [12,17]. Note that $\theta = ds/R = cds$, therefore, the work performed to produce a curvature c in the membrane segment is $dW = m_p cds/2$.

We assume that the viral membrane is incompressible and it can resist bending. The shape of the membrane is determined by minimizing a Helfrich-type energy functional in addition to the energy induced by the protein bending moment. The energy functional takes the form

$$E = \frac{1}{2}k_b \int (c - c_0)^2 ds + \frac{1}{2} \int m_p cds. \quad (2.1)$$

Here the first term is the Helfrich energy [15] due to the bending rigidity of the membrane. The last term is an energy contribution due to the work done by the HA protein. k_b is the bending rigidity and c_0 denotes the spontaneous curvature, which takes the

possible asymmetry of the bilayer into account.

3 Model Analysis

In this section, we derive the formulas for the tension and the bending moment developed in the membrane. We also analyze the equilibrium shape of the membrane.

3.1 Membrane tension

Let \vec{r} be the position of point particles along the membrane. Then we can express curvature c in the following form.

$$c = \left| \frac{d^2\vec{r}}{ds^2} \right| = \left(\frac{d^2\vec{r}}{ds^2} \cdot \frac{d^2\vec{r}}{ds^2} \right)^{1/2}.$$

The energy functional can be written as

$$E = \frac{k_b}{2} \int \left(\frac{d^2\vec{r}}{ds^2} \cdot \frac{d^2\vec{r}}{ds^2} \right) ds + \int \left(\frac{m_p}{2} - k_b c_0 \right) \left(\frac{d^2\vec{r}}{ds^2} \cdot \frac{d^2\vec{r}}{ds^2} \right)^{1/2} ds + \frac{k_b}{2} \int c_0^2 ds.$$

We assume $\delta\vec{r}$ to be an infinitesimal virtual displacement. For two-dimensional incompressible membrane, the arc length between any two point particles along the membrane is preserved, i.e., $\delta(ds) = 0$. This induces the energy variation

$$\delta E = \int \left[k_b \frac{d^2\vec{r}}{ds^2} \cdot \frac{d^2\delta\vec{r}}{ds^2} + \left(\frac{m_p - 2k_b c_0}{2c} \right) \frac{d^2\vec{r}}{ds^2} \cdot \frac{d^2\delta\vec{r}}{ds^2} \right] ds.$$

Performing integration by parts twice and simplifying, we obtain

$$\delta E = - \int \frac{d}{ds} \left[\left(k_b c^2 + \frac{m_p - 2k_b c_0}{2} c \right) \vec{t} + \left(k_b \frac{dc}{ds} + \frac{1}{2} \frac{d(m_p - 2k_b c_0)}{ds} \right) \vec{n} \right] \cdot \delta\vec{r} ds, \quad (3.1)$$

where \vec{n} and \vec{t} are the unit normal and the unit tangential vector respectively.

Membrane incompressibility for a two-dimension membrane implies [27],

$$\vec{t} \cdot \frac{d\delta\vec{r}}{ds} = 0, \quad (3.2)$$

which leads to

$$\int \frac{d}{ds} (\lambda \vec{t}) \cdot \delta\vec{r} ds = 0, \quad (3.3)$$

where λ is an arbitrary function. Therefore, we can add $\int d(\lambda \vec{t})/ds \cdot \delta\vec{r} ds$ to (3.1), which gives

$$\delta E = - \int \frac{d}{ds} \left[\left(k_b c^2 + \frac{m_p - 2k_b c_0}{2} c + \lambda \right) \vec{t} + \left(k_b \frac{dc}{ds} + \frac{1}{2} \frac{d(m_p - 2k_b c_0)}{ds} \right) \vec{n} \right] \cdot \delta\vec{r} ds. \quad (3.4)$$

Writing the membrane load as $\vec{\mathcal{F}} = \vec{\mathcal{F}}^n \vec{n} + \vec{\mathcal{F}}^t \vec{t}$, the principle of virtual displacements gives [27]

$$\delta E = - \int \vec{\mathcal{F}} \cdot \delta \vec{r} ds. \quad (3.5)$$

Comparing equation (3.4) and equation (3.5), we obtain the membrane load

$$\vec{\mathcal{F}} = \frac{d}{ds} \left[\left(k_b c^2 + \frac{m_p - 2k_b c_0}{2} c + \lambda \right) \vec{t} + \left(k_b \frac{dc}{ds} + \frac{1}{2} \frac{d(m_p - 2k_b c_0)}{ds} \right) \vec{n} \right]. \quad (3.6)$$

Let τ , σ and m be the in-plane tension, transverse shear tension, and bending moment developed in the membrane due to deformation, respectively. The tension exerted on a cross section of the membrane is

$$\vec{\mathcal{T}} = \tau \vec{t} + \sigma \vec{n}.$$

Therefore, the total force over an infinitesimal section of the membrane is given by

$$\vec{\mathcal{F}} = \frac{d\vec{\mathcal{T}}}{ds} = \frac{d}{ds} (\tau \vec{t} + \sigma \vec{n}). \quad (3.7)$$

Comparing equation (3.6) and equation (3.7), we obtain

$$\tau = k_b c^2 + \frac{c}{2} (m_p - 2k_b c_0) + \lambda, \quad (3.8a)$$

$$\sigma = k_b \frac{dc}{ds} + \frac{1}{2} \frac{d}{ds} (m_p - 2k_b c_0). \quad (3.8b)$$

3.2 Spontaneous curvature

Spontaneous curvature c_0 is caused by asymmetry in the lipid bilayer, e.g., due to the shape of lipid molecules or imbedded proteins [5, 26]. It has been suggested, cf. [8], that membrane fusion and fission could be a consequence of membrane re-modelling, i.e., change of spontaneous curvature by the action of protein molecules. It can be observed from (3.8) that the spontaneous curvature and protein induced bending moment m_p have similar effects on the membrane tension. In fact, based on the force alone, one can argue that these two quantities are equivalent if the induced spontaneous curvature change is given by

$$c_{0,p} = -\frac{m_p}{2k_b}.$$

In this case, the protein induced bending moment m_p can be replaced by $c_{0,p}$ and the total spontaneous curvature is $c_0 + c_{0,p}$. However, the energy stored in the membrane are not the same, c.f. (2.1). Therefore, the mechanism for protein-mediated viral membrane fusion due to bending moment m_p differs from the effect of spontaneous curvature.

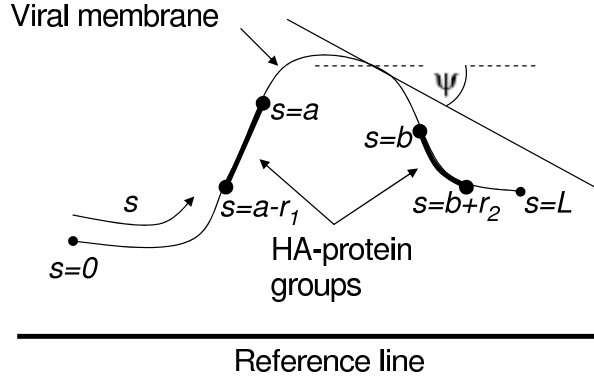


Figure 2: Viral membrane of length L with two groups of protein located from $s = a - r_1$ to $s = a$ and $s = b$ to $s = b + r_2$. ψ is the angle between the tangent line and a horizontal reference line.

3.3 Equilibrium shape equation

We now obtain the equilibrium shape equations of two dimensional membrane by performing the force and the torque balance over an infinitesimal section of the membrane. From equation (3.7), in the absence of any other forces except the protein force, force balance in tangential and normal direction along with the torque balance provides us with the following equilibrium shape equations [22]:

$$\frac{d\tau}{ds} + c\sigma = 0, \quad (3.9a)$$

$$\frac{d\sigma}{ds} - c\tau = 0, \quad (3.9b)$$

$$\frac{dm}{ds} - \sigma = 0. \quad (3.9c)$$

We now consider a membrane segment of length L as shown in Fig. 2. To represent membrane segments both with and without HA-protein cluster, we have considered two HA-protein clusters. However, the method discussed here can easily be extended to a membrane containing more than two protein groups. Let ψ be the angle made by the tangent to the curve with a line parallel to a reference line. Then we can express the curvature as

$$c = \frac{d\psi}{ds}. \quad (3.10)$$

We further assume that the reference line is parallel to the x-axis of the Cartesian coordinate system. Then Cartesian coordinates (x, y) of points in the membrane can be obtained by solving the following system of differential equations:

$$\frac{dx}{ds} = \cos \psi, \quad x(0) = x_0, \quad (3.11a)$$

$$\frac{dy}{ds} = -\sin \psi, \quad y(0) = y_0, \quad (3.11b)$$

where (x_0, y_0) is an arbitrary point fixed to correspond to the point $s = 0$ of the membrane. By solving equations (3.9a)-(3.11b) together with relations (3.8) and with proper boundary conditions we have the equilibrium shape of the membrane.

3.4 Boundary conditions

To solve the shape equations, we need to impose proper boundary conditions. Total membrane arc-length is chosen sufficiently large such that the membrane remains undisturbed (i.e. parallel to reference line) at the boundaries. In this case, we have $\psi(0) = \psi(L) = 0$. We further assume a constant in-plane tension $\tau = \tau_0$ at the boundary $s = L$, which depends upon the environment where the membrane is located. As we take the membrane sufficiently large so as to make $s = L$ undisturbed, we further fix the vertical position of the membrane end $s = L$ from the planar state by taking $y = y_L$ at $s = L$. Therefore, to solve the system (3.9)-(3.11) we use the following set of boundary conditions.

$$s = 0 : \quad \psi = 0, \quad x = x_0, \quad y = y_0, \quad (3.12a)$$

$$s = L : \quad \psi = 0, \quad \tau = \tau_0, \quad y = y_L. \quad (3.12b)$$

3.5 Bending moment due to HA-protein

At low pH values, multiple HA trimers assemble around the fusion site to perform concerted activation to synchronously release the conformational energy [24]. These assembled HA trimers can be assumed to form clusters surrounding the fusion site [1, 4, 9, 16, 18, 20, 31, 37]. Moreover, fusion peptide interaction among neighboring HAs has been hypothesized to be responsible for a measurable decrease in the lateral mobility of HA after activation [14, 24]. Based on these observations, for our simple two-dimensional model, we assume that two protein groups of size r_1 and r_2 are acting at positions $a - r_1 < s < a$ and $b < s < b + r_2$, respectively with a separation $b - a$ between them (Fig. 2). We, therefore, assume that the bending moment m_p exerted by the protein is given by

$$m_p(s) = \begin{cases} 0, & 0 \leq s < a - r_1; \\ M_p^1, & a - r_1 < s < a; \\ 0, & a < s < b; \\ M_p^2, & b < s < b + r_2; \\ 0, & b + r_2 < s \leq L. \end{cases} \quad (3.13)$$

3.6 Membrane torque

From the torque balance

$$\frac{dm}{ds} = \sigma, \quad (3.14)$$

we obtain

$$m = k_b(c - c_0) + \frac{m_p}{2} + C, \quad (3.15)$$

where C is an integrating constant. In the absence of HA-protein, we assume that the membrane takes the shape given by its spontaneous curvature c_0 , in which the bending moment m vanishes. Therefore, when $m_p = 0$, $c = c_0$ and $m = 0$. This implies $C = 0$. Then equation (3.15) gives total bending moment developed in the membrane

$$m = k_b(c - c_0) + \frac{m_p}{2}. \quad (3.16)$$

When $m_p = 0$, the bending moment reduces to $m = k_b(c - c_0)$, which is consistent with the constitutive equation showing the linear relation between bending moment and the curvature as explained in [27].

3.7 Tensionless membrane

Because of complexity of the model, to analytically understand the role of HA-protein in deforming membrane, we consider a special case. When both the in-plane tension and the transverse shear tension vanish (i.e. $\tau = \sigma = 0$), we have

$$\lambda + k_b c^2 + \frac{m_p - 2k_b c_0}{2} c = 0, \quad (3.17a)$$

$$\frac{d}{ds} \left(2k_b \frac{d\psi}{ds} - 2k_b c_0 + m_p(s) \right) = 0. \quad (3.17b)$$

Integrating equation (3.17b) once, we obtain

$$\frac{d\psi}{ds} = -\frac{1}{2k_b} m_p(s) + C, \quad (3.18)$$

where $C = c_0 + \mathcal{K}/(2k_b)$ with integrating constant \mathcal{K} .

Since $m_p(s)$ is piecewise constant, we can obtain an analytical solution by integrating equation (3.18). We solve equation (3.18) for $0 \leq s < a - r_1$ with $\psi(0) = 0$. Imposing continuity of ψ , we further solve equation (3.18) piecewise for $a - r_1 \leq s < a$, $a \leq s < b$, $b \leq s < b + r_2$ and $b + r_2 \leq s \leq L$. Finally, using the boundary condition $\psi(L) = 0$, we obtain the solution of equation (3.18) as follows:

$$\psi(s) = \begin{cases} -Q_1 s, & 0 \leq s < a - r_1; \\ Q_2 s - P_2, & a - r_1 \leq s < a; \\ -Q_3 s + P_3, & a \leq s < b; \\ Q_4 s + P_4, & b \leq s < b + r_2; \\ -Q_5 s + P_5, & b + r_2 \leq s \leq L, \end{cases} \quad (3.19)$$

where

$$Q_1 = Q_3 = Q_5 = -C, \quad Q_2 = -\frac{M_p^1}{2k_b} + C, \quad Q_4 = -\frac{M_p^2}{2k_b} + C,$$

$$P_2 = -\frac{M_p^1(a-r_1)}{2k_b}, \quad P_3 = -\frac{M_p^1 r_1}{2k_b}, \quad P_4 = -\frac{M_p^1 r_1 - M_p^2 b}{2k_b}, \quad P_5 = -LC.$$

Clearly, in the absence of protein (i.e. $M_p^1 = M_p^2 = 0$), all P 's and Q 's become zero. This results in $\psi = 0$, corresponding to the undeformed membrane. Moreover, substituting $\psi(s)$ in energy functional (2.1) and integrating, the minimum energy of the membrane is obtained as follows

$$E_{min} = \frac{k_b}{2} [(a-r_1)(Q_1+c_0)^2 + r_1(Q_2-c_0)^2 + (b-a)(Q_3+c_0)^2 + r_2(Q_4-c_0)^2 + (L-b-r_2)(Q_5+c_0)^2] + \frac{1}{2} [M_p^1 r_1 Q_2 + M_p^2 r_2 Q_4]. \quad (3.20)$$

Similarly, integrating in the interval $a < s < b$, we obtain the energy stored inside two regions where the protein exert bending moments

$$E_{min}^{int} = \frac{k_b}{2} (b-a)(Q_3+c_0)^2. \quad (3.21)$$

We can see that E_{min}^{int} is directly proportional to the bending moments M_p^1, M_p^2 as well as the protein sizes r_1, r_2 . This is consistent with the results obtained in [18,36].

The shape of the membrane can be obtained by solving (3.11) and the position of the membrane is given in Appendix.

4 Results and Discussion

In reality, the total arc length L of the membrane segment, with both ends undisturbed (flat), depends upon the density of the activated HA trimers. Based on the fact that the contact area of a radius ~ 25 nm can have ~ 10 dimples if all the HA molecules in this area are activated [18], it has been estimated in [36] that the radius of circular undisturbed membrane is 20 nm. Therefore, we take $L = 40$ nm (the diameter of the circular membrane) for the computation of our two dimensional model. Moreover, for all computations, the bending rigidity is given as $k_b = 20kT$ as in [18,36] where k is the Boltzman constant and T is the absolute temperature. All computations are carried out by choosing the normal human body temperature i.e. 310.15 K. Numerical solutions are obtained by solving the shape equations with the tool *bvp4c.m* in MATLAB. *bvp4c.m* solves the boundary value problems for ordinary differential equations by using a finite difference code that implements the three-stage Lobatto IIIa formula.

4.1 Tensionless membrane

We first compare our numerical result with the analytical result obtained for the tensionless membrane. For this purpose, we take $\tau_0 = 0 \text{ Nm}^{-1}$. The numerical solution of the system (3.9)-(3.11) with boundary condition (3.12) is compared with the analytical one given by (5.1) in Fig. 3(a) for the parameter set $M_p^1 = M_p^2 = -2.4 \times 10^{-11} \text{ N}$,

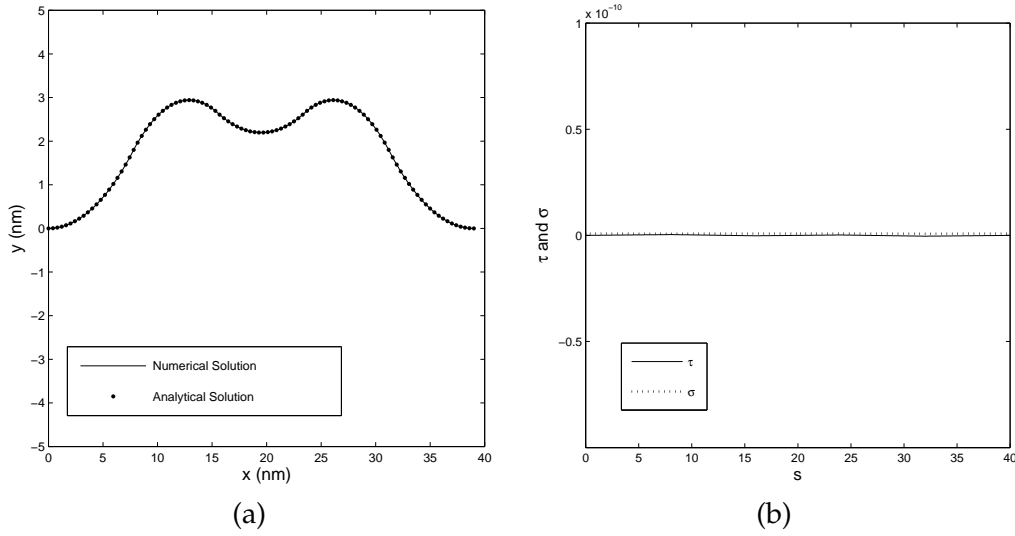


Figure 3: (a) Comparison of numerical and analytical solution of the membrane shape. (b) Computed τ and σ in the membrane.

$c_0 = 0$, $r_1 = r_2 = b - a = 8$ nm, $a = 16$ nm and $x_0 = y_0 = y_L = 0$. It can clearly be seen that the two results perfectly agree with each other. We have also plotted the computed values of τ and σ in the membrane, cf. Fig. 3(b), which shows that the membrane is indeed tensionless. Therefore, for $\tau_0 = 0$, we have verified that $\tau = \sigma = 0$ is the solution to (3.9)-(3.11).

In Fig. 4, we plot the shape of the membrane for various protein bending moments M_p^1 ($= M_p^2$), various protein size r_1 ($= r_2$) and various separation distance ($b - a$) of the two protein groups. Due to the bending moments exerted by HA protein, the membrane deforms and forms dimples, similar to the axis-symmetric case [36]. It can be seen that the height of the dimple increases with an increase in the magnitude of the bending moments, which is consistent with the result obtained in [18,36]. It seems that there exists an optimal size of HA-protein groups to produce a maximum height of the dimple, see Fig. 4(b). In Fig. 4(c), the results show that the size of dimple grows as $b - a$ decreases, i.e., when the two groups of proteins move closer.

The energy in the entire membrane and the energy inside two protein groups against the magnitude of M_p^1 ($= M_p^2$) and r_1 ($= r_2$) are plotted in Fig. 5. Energy in the entire membrane is calculated by integrating functional (2.1) from $s = 0$ to $s = L$ and the energy inside the two protein groups is calculated by integrating from $s = a$ to $s = b$. The analytical expressions for tensionless membrane are given by equations (3.20) and (3.21), respectively. Both the total energy in its absolute value and the energy between two protein groups increase as the magnitude of the bending moments and the size of the protein groups increase. These results are consistent with the results obtained in [18,36]. However, the magnitude of the energy stored in the two-dimensional membrane is less than that in axisymmetric case, cf. Figures 6 and 7 in [36]. The energy level (< 1 kT) stored due to linear HA-protein clusters considered

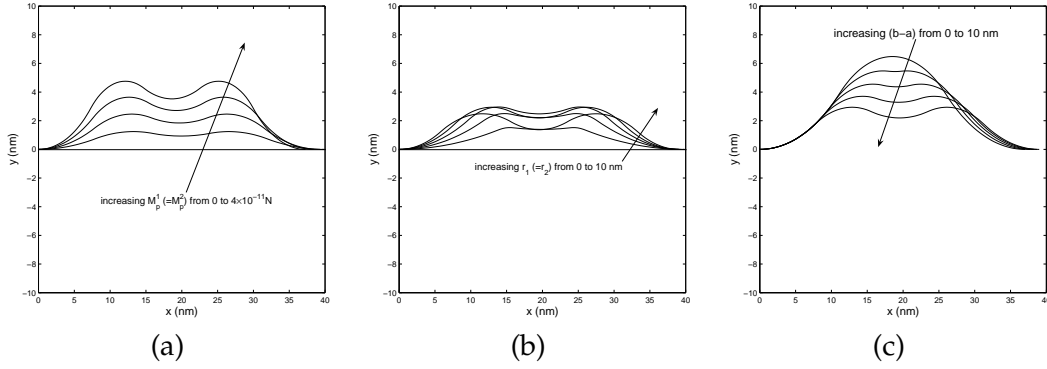


Figure 4: Shape of the membrane under various conditions. (a) $M_p^1 (= M_p^2)$ varies from 0 to -4×10^{-11} N while fixing $c_0 = 0$, $r_1 = r_2 = b - a = 8$ nm and $a = 16$ nm; (b) $r_1 (=r_2)$ varies from 0 nm to 10 nm while fixing $c_0 = 0$, $M_p^1 = M_p^2 = -2.4 \times 10^{-11}$ N; (c) The separation distance $(b - a)$ of the two protein groups varies from 0 nm to 10 nm while fixing $c_0 = 0$, $M_p^1 = M_p^2 = -2.4 \times 10^{-11}$ N and $r_1 = r_2 = 8$ nm.

here is not enough to overcome an energy barrier of ≈ 37 kT for the merging of monolayers [19, 23] required for a successful fusion. This shows that linear HA-protein clusters are not favorable for membrane fusion compared to axisymmetric clusters supporting the hypothesis in [18, 36].

We now examine more closely the effects of HA bending moment and the size of HA protein group on membrane deformation. For simplicity, we set $a = L/2 - \delta$ and $b = L/2 + \delta$ with a separation 2δ between the two groups of proteins consider the symmetrical protein case, i.e. $M_p^1 = M_p^2 = M_p$ and $r_1 = r_2 = r$. For non-zero value of M_p , y -equation (See Appendix) shows that changing the sign of M_p leads to the sign change in P 's and Q 's and also in y while the position (measured by x) remains unchanged. This indicates the amount of deformation of the membrane is the same and in opposite directions for $\pm M_p$. Assuming that the relevant direction is in the positive direction of y (i.e., the host cell membrane lies above the viral membrane), in the rest of the paper, we present the results for $M_p \leq 0$.

From (3.19), it is straightforward to verify that the curvature of the membrane is given by

$$c = \frac{d\psi}{ds} = \begin{cases} -Q_1, & 0 \leq s < a - r_1; \\ Q_2, & a - r_1 < s < a; \\ -Q_3, & a < s < b; \\ Q_4, & b < s < b + r_2; \\ -Q_5, & b + r_2 < s \leq L. \end{cases} \quad (4.1)$$

As Q_i for $i = 1$ to $i = 5$ are all constants, we conclude that the membrane consists of circular arcs. Using (3.11a) and (3.11b), we get $dy/dx = -\tan \psi$, which provides the three critical points of the membrane $y(x)$ as

$$s_1 = \frac{L}{L - 2r} \left(\frac{L}{2} - \delta + r \right), \quad s_2 = \frac{L}{2}, \quad s_3 = \frac{L}{L - 2r} \left(\frac{L}{2} + \delta - r \right).$$

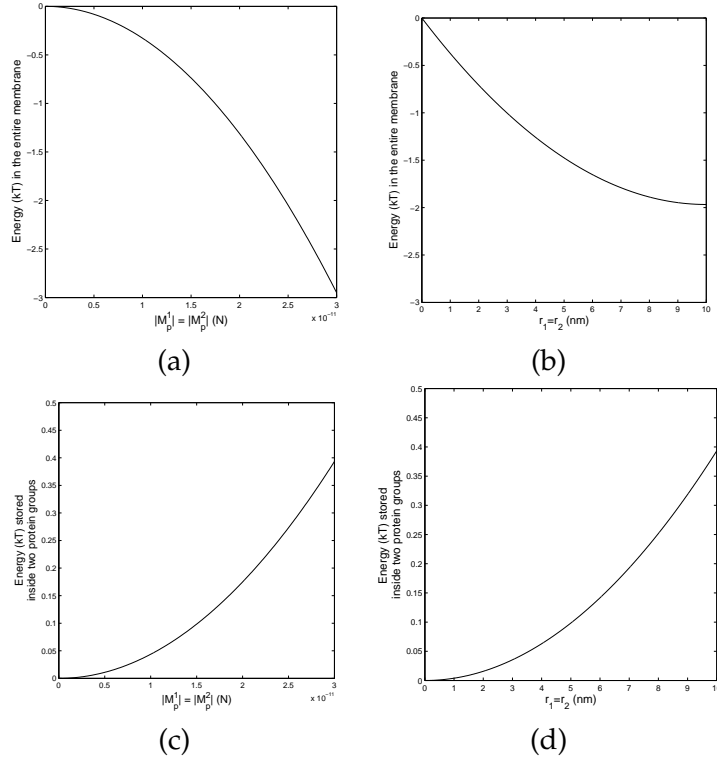


Figure 5: (a) Energy in the entire membrane affected by the bending moments exerted by HA protein ($M_p^1 = M_p^2$), (b) Energy in the entire membrane affected by the size of HA protein ($r_1 = r_2$), (c) Energy stored inside two protein groups affected by the bending moments exerted by HA protein ($M_p^1 = M_p^2$), and (d) Energy stored inside two protein groups affected by the size of HA protein ($r_1 = r_2$).

Using $d^2y/dx^2 = -\sec^3 \psi (d\psi/ds)$, it is straightforward to verify that

$$\left. \frac{d^2y}{dx^2} \right|_{s=s_1, s_3} < 0, \quad \left. \frac{d^2y}{dx^2} \right|_{s=s_2} > 0.$$

Therefore, membrane height $y(x)$ has two local maxima at $s = s_1$ and $s = s_3$ and a local minimum at $s = s_2$, occurred in the centers of the circular arcs given by (4.1).

When δ decreases, i.e., when two protein groups move closer, we find that s_1 increases and s_3 decreases while s_2 remains unaffected. In the limit of $\delta \rightarrow 0$, the three critical points collapse into a single point $s_1 = s_2 = s_3 = L/2$ where d^2y/dx^2 is negative. The dimple top is located in the center, remains circular, and budding upwards. In this case, the deformation of the two-dimensional and axisymmetric membranes are similar except that it is circular in 2D but non-spherical in the axisymmetrical setting.

Let h be the membrane height in the center ($s = L/2$), which is given by

$$h = \frac{1 - \cos(Q_1(a - r))}{Q_1} + \frac{\cos(Q_2a - P_2) - \cos(Q_2(a - r) - P_2)}{Q_2} + \frac{\cos(Q_3a - P_3) - \cos(0.5Q_3L - P_3)}{Q_3}. \quad (4.2)$$

We have plotted h as a function of M_p and r in Figs 6(a) and (b), respectively. It can be seen that h is a monotonic function of M_p . However, there exists a critical value of r which gives a maximal h . The critical value can be obtained as $r = a - L/4$ and it can be verified that d^2h/dr^2 is negative at $r = a - L/4$.

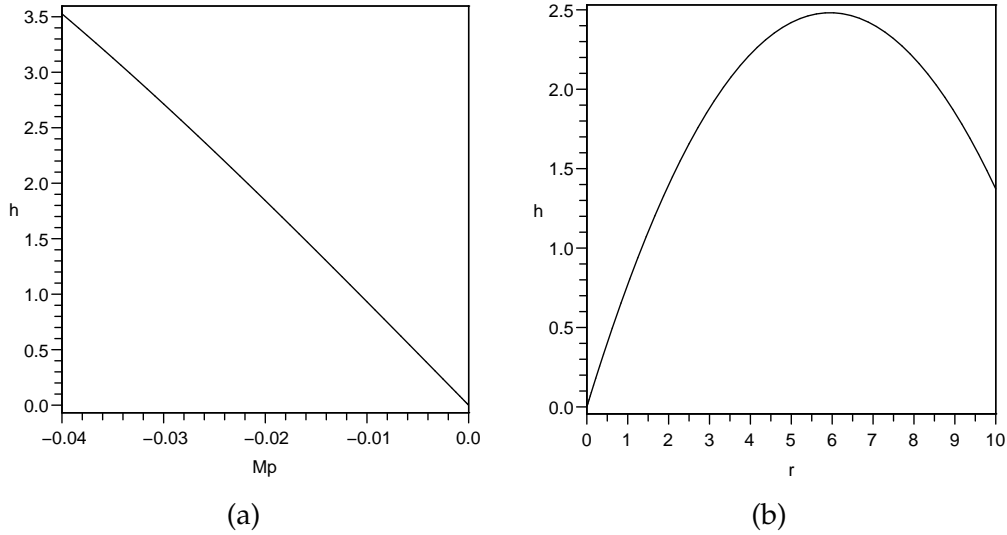


Figure 6: Height of membrane at the center (a) as a function of bending moment exerted by protein and (b) as a function of the size of protein group. Here, the unit of h and r is nm and the unit of M_p is 10^{-9} N.

4.2 Membrane under tension

In this section, we observe the effect of *a priori* in-plane tension on the shape of the membrane. We create the in-plane tension in the membrane by imposing the non-zero value of τ_0 , which is the in-plane tension at the boundary $s = L$. We also applied non-zero tension at the boundary $s = 0$, the similar results were obtained. We examine the effect of *a priori* in-plane tension by increasing τ_0 from 0 to 1×10^{-2} Nm^{-1} while keeping $M_p^1 = M_p^2 = -2.4 \times 10^{-11}$ N, $c_0 = 0$, $r_1 = r_2 = b - a = 8$ nm, and $a = 16$ nm. Fig. 7(a) shows that an increase in tension in the membrane reduces the dimple height. Therefore, membrane tension opposes the formation of dimple. Our result is consistent with the experimental observation in [25], where it was shown that membrane tension prevents dimple formation and inhibits fusion.

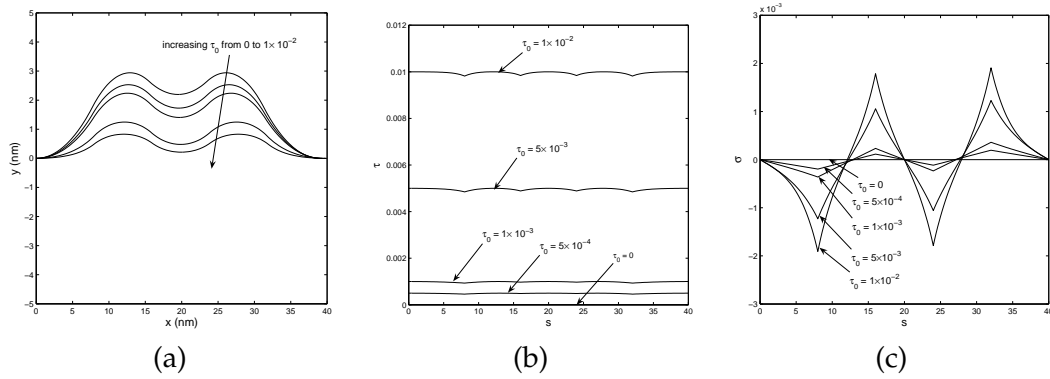


Figure 7: (a) Shape of the membrane, (b) in-plane tension, and (c) transverse shear tension in the membrane with a priori tension.

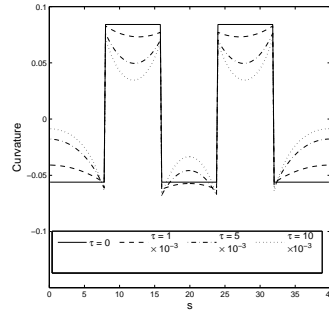


Figure 8: Curvatures of the membrane under a priori tension.

The distribution of in-plane tension and transverse shear tension in the membrane are shown in Figs. 7(b) and (c), respectively. For each τ_0 , the in-plane tension remains almost uniform throughout the membrane with the magnitude close to τ_0 (Fig. 7(b)). Therefore, *a priori* tension is very important for the dimple formation. As shown in Fig. 7(c), the transverse shear tension, however, is not uniform in the membrane. Instead it is distributed in a zigzag manner. In fact, it increases in the region where protein resides and decreases where the protein is absent. An increase in τ_0 has a positive effect on the transverse tension.

Finally we note that for membrane under priori tension, its shape deviates from that of a tensionless membrane. As shown in Figure 8, the curvature is no longer piecewise constants, which indicates that the dimples are not circular arcs.

4.3 Asymmetrical protein force

So far we have discussed the case when two protein groups are symmetric (i.e. $M_p^1 = M_p^2$ and $r_1 = r_2$). We now examine how the asymmetric properties of two HA-protein groups affect the shape of the membrane. In Fig. 9, we plot the shape of the membrane

for two protein groups of different sizes (i.e. $r_1 \neq r_2$) and bending moments (i.e. $M_p^1 \neq M_p^2$). We take the different combination of the magnitude of M_p^1 and M_p^2 within the range 0 to 2.4×10^{-11} N in Fig. 9(a) and the different combination of r_1 and r_2 within the range 0 to 8 nm in Fig. 9(b). As seen in Fig. 9(a), the dimple shape does not grow symmetrically if the two protein groups apply different bending moments. The size of the membrane dimpling is higher towards the protein group exerting bending moment of higher magnitude. A similar effect on the membrane shape can be seen due to the different size of two protein groups (See Fig. 9(b)). When the HA-protein in the membrane form two groups of different size, the membrane forms asymmetric dimple with higher dimpling towards the protein group of larger size, as expected.

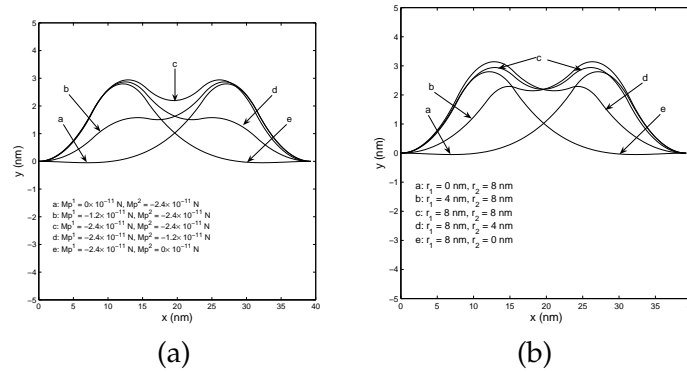


Figure 9: Shape of the membrane affected by (a) bending moments exerted by HA protein ($M_p^1 \neq M_p^2$), and (b) size of HA protein ($r_1 \neq r_2$).

4.4 Axisymmetric vs. linear HA-protein clusters

We now compare the effect of linear HA-protein clusters presented in this study with the effect of axisymmetric HA-protein clusters [18, 36] on membrane deformation and budding related to fusion.

Both axisymmetric and linear HA-protein clusters have potential for membrane budding and dimple formation. In both cases, the height of dimples increases with an increase in the magnitude of the bending moment exerted by the protein and decreases with an increase in tension in the membrane. Moreover, energy in the membrane increases as the magnitude of the bending moment and the size of the protein clusters increase in both axisymmetric and linear cases.

Even though the membrane dimples are possible to be generated by both clusters, shape of a two-dimensional membrane is quite different from that of an axisymmetric one, where the dimple top (maximum height) occurs in the center and its shape is in general non-spherical. In two-dimensional membrane, the dimple tops occur in pair and are not in the center in general. However, the shapes of the dimples are circular. The dimple height monotonically increases with respect to size of axisymmetric

HA-protein clusters while there exists an optimal size of linear HA-protein clusters to produce a maximum dimple height.

More importantly, the magnitude of the energy stored in the membrane deformed due to linear HA-protein clusters is significantly lower than in the membrane deformed due to axisymmetric HA-protein clusters. In order to facilitate fusion, a significant amount of energy must be available for the monolayers to overcome an energy barrier and merge. The energy level in axisymmetric case is in accordance with the energy barrier of $\approx 37kT$ for the merging of monolayers [19,23,36] while the energy level in linear case is quite low. Therefore, even though membrane deformation and budding is possible due to both axisymmetric and linear HA-protein clusters, our results show that the HA-protein clusters of axisymmetric structure are much more favorable for a successful membrane fusion and viral infection.

5 Conclusion

Experimental evidence shows that Hemagglutinin (HA) protein clustered in linear structure can cause a successful influenza virus budding from a thin section of membrane (approximately two-dimensional membrane). Identifying these novel experimental observations, in this paper we study a two-dimensional model to understand the role of linearly clustered HA-protein on the influenza viral membrane deformation. We calculate tension and bending moment developed in the membrane. We derive the shape equation of the equilibrium membrane from force and torque balance. For tensionless membranes, we provide explicit formulas for the deformed membrane shape and associated energy under the influence of two protein groups. Our numerical and analytical solutions confirm the formation of dimples caused by HA-protein, which was hypothesized in the literature and observed experimentally. By utilizing the analytical solution for tensionless membranes, we show that in this case membrane deforms into a patch of circular arcs in the two dimensional setting with maximum deformation occurred away from the center. This is different from the axisymmetric case where the maximum height always occurs in the center while the dimple shape is non-spherical [36].

Our results also show that the energy and the size of the membrane dimple are proportional to the bending moment exerted by the protein as well as size of the protein groups. *A priori* membrane tension makes it difficult for the membrane to form dimples, which is consistent with experimental observations. The dimple shape is not symmetric about the center of the membrane when the two protein groups differ in size or exert different bending moments.

Unlike in axisymmetric HA-protein clusters, where the level of energy stored in the membrane is in accordance with the energy barrier for membrane merging required for a successful fusion, the energy stored in the membrane due to linear HA-protein clusters is significantly low. Therefore, the linear HA-protein clusters are not favorable to bring a successful fusion, despite their capability for membrane deformation and

budding.

Acknowledgement. This research was supported by the Susan Mann Dissertation Scholarship Award of York University; the Natural Science and Engineering Research Council (NSERC) of Canada; and Mathematics for Information Technology and Complex System (MITACS) of Canada.

References

- [1] J. Bentz and H. Ellens, An architecture for the fusion site of influenza hemagglutinin, *FEBS Lett.* 276(1990) 1-5.
- [2] J. Bentz, Membrane fusion mediated by coiled coils: a hypothesis, *Biophys. J.* 78(2000) 886-900.
- [3] R. Blumenthal, M. J. Clague, S. R. Durell and R. M. Eppard, Membrane fusion, *Chem. Rev.* 103(2003) 53-69.
- [4] R. Blumenthal, C. C. Pak, Y. Raviv, M. Krumbiegel, L. D. Bergelson, S. J. Morris, and R. J. Lowy, Transient domains induced by influenza hemagglutinin during membrane fusion, *Mol. Membr. Biol.* 12(1995) 135-142.
- [5] D. Boal, *Mechanics of the cell*, Cambridge University Press, Cambridge, UK (2002).
- [6] P. A. Bullough, F. M. Hughson, J. J. Skehel and D. C. Willey, Structure of influenza hemagglutinin at the pH of membrane fusion, *Nature* 371 (1994) 37-43.
- [7] C. M. Carr and P. S. Kim, A spring-loaded mechanism for the conformational change of influenza hemagglutinin, *Cell* 73 (1993) 823-832.
- [8] L. V. Chernomordik and M. M. Kozlov, Protein-lipid interplay in fusion and fission of biological membranes, *Annu. Rev. Biochem.* 72(2003) 175-207.
- [9] T. Danieli, S. L. Pelletier, Y. I. Henis and J. M. White, Membrane fusion mediated by the influenza virus hemagglutinin requires the concerted action of at least three hemagglutinin trimers, *J. Cell Biol.* 133 (1996) 559-569.
- [10] D. C. Ekiert, G. Bhabha, M. Elsliger, R. H. E. Friesen, M. Jongeneelen, M. Throsby, J. Goudsmit and I. A. Wilson, Antibody recognition of a highly conserved influenza virus epitope, *Science* (2009) (online <http://www.sciencemag.org/cgi/content/abstract/1171491>).
- [11] Y. Gaudin, R. W. H. Ruigrok and J. Brunner, Low-pH induced conformational changes in viral fusion proteins: implications for the fusion mechanism, *J. Gen. Virol.* 76 (1995) 1541-1556.
- [12] J. M. Gere, *Mechanics of Materials*, Brooks/Cole-Thomson Learning, Belmont, CA, USA (2004).
- [13] J. A. Gruenke, R. T. Armstrong, W. W. Newcomb, J. C. Brown and J. M. White, New insights into the spring-loaded conformational change of influenza virus hemagglutinin, *J. Virol.* 76 (2002) 4456-4466.
- [14] O. Gutman, T. Danieli, J. M. White and Y. I. Henis, Effects of exposure to low pH on the lateral mobility of influenza hemagglutinin expressed at the cell surface: correlation between mobility inhibition and inactivation, *Biochem.* 32 (1993) 101-106.
- [15] W. Helfrich, Elastic properties of lipid bilayers: theory and possible experiments, *Z. Naturforsch C* 28 (1973) 693-703.
- [16] S. T. Hess, M. Kumar, A. Verma, J. Farrington, A. Kenworthy and J. Zimmerberg, Quantitative electron microscopy and fluorescence spectroscopy of the membrane distribution of influenza hemagglutinin, *J. Cell Biol.* 169 (2005) 965-976.

- [17] R. C. Hibbeler, *Mechanics of materials*, Pearson Prentice Hall, Upper Saddle River, NJ, USA, (2005).
- [18] M. M. Kozlov and L. V. Chernomordik, A mechanism of protein-mediated fusion: coupling between refolding of the influenza hemagglutinin and lipid rearrangements, *Biophys. J.* 75 (1998) 1384-1396.
- [19] P. I. Kuzmin, J. Zimmerberg, Y. A. Chizmadzhev and F. S. Cohen, A quantitative model for membrane fusion based on low-energy intermediates, *PNAS* 98 (2001) 7235-7240.
- [20] G. P. Leser and R. A. Lamb, Influenza virus assembly and budding in raft-derived microdomains: a quantitative analysis of the surface distribution of HA, NA and M2 proteins, *Virology* 342 (2005) 215-227.
- [21] Y. Li, X. Han, A. L. Lai, J. H. Bushweller, D. S. Cafiso and L. K. Tamm, Membrane structures of the hemifusion-inducing fusion peptide mutant G1S and the fusion-blocking mutant G1V of influenza virus hemagglutinin suggest a mechanism for pore opening in membrane fusion, *J. Virol.* 79 (2005) 12065-12076.
- [22] A. E. H. Love, *Treatise on the mathematical theory of elasticity*, 4th Edd., Courier Dover Publications, USA (1944).
- [23] V. S. Markin and J. P. Albanesi, Membrane fusion: stalk model revisited, *Biophys. J.* 82 (2002) 693-712.
- [24] I. Markovic, E. Leikina, M. Zhukovsky, J. Zimmerberg and L. V. Chernomordik, Synchronized activation and refolding of influenza hemagglutinin in multimeric fusion machines, *J. Cell Biol.* 155 (2001) 833-843.
- [25] R. M. Markosyan, G. B. Melikyan and F. S. Cohen, Tension of membranes expressing the Hemagglutinin of influenza virus inhibits fusion, *Biophys. J.* 77 (1999) 943-952.
- [26] C. M. Marques and J. B. Fournier, Deviatoric spontaneous curvature of lipid membranes induced by Siamese macromolecular cosurfactants, *Europhys. Lett.* 35(1996) 361-365.
- [27] C. Pozrikidis, Shell theory for capsules and cells. In *Modeling and Simulation of Capsules and Biological Cells*, Ed. C. Pozrikidis, Chapman and Hall/CRC, Boca Raton, FL, USA (2003) 35-101.
- [28] J. J. Skehel and D. C. Wiley, Receptor binding and membrane fusion in virus entry: the influenza haemagglutinin, *Ann. Rev. Biochem.* 69 (2000) 531-569.
- [29] T. Stegmann, Influenza hemagglutinin-mediated membrane fusion does not involve inverted phase lipid intermediates, *J. Biol. Chem.* 268 (1993) 1716-1722.
- [30] J. Sui, W. C. Hwang, S. Perez, G. Wei, D. Aird, L. Chen, E. Santelli, B. S., G. Cadwell, M. Ali, H. Wan, A. Murakami, A. Yammanuru, T. Han, N. J. Cox, L. A. Bankston, R. O. Donis, R. C. Liddington and W. A. Marasco, Structural and functional bases for broad-spectrum neutralization of avian and human influenza A viruses, *Nat. Struct. Mol. Biol.* 16 (2009) 265-273.
- [31] M. Takeda, G. P. Leser, C. J. Russell, and R. A. Lamb, Influenza virus hemagglutinin concentrates in lipid raft microdomains for efficient viral fusion, *PNAS* 100 (2003) 14610-14617.
- [32] L. K. Tamm, F. Abildgaard, A. Arora, H. Blad and J. H. Bushweller, Structure, dynamics and function of the outer membrane protein A (OmpA) and influenza hemagglutinin fusion domain in detergent micelles by solution NMR, *FEBS Lett.* 555 (2003) 139-143.
- [33] L. K. Tamm, Hypothesis: spring-loaded boomerang mechanism of influenza hemagglutinin-mediated membrane fusion, *Biochem. et Biophys. Acta* 1614 (2003) 14-23.
- [34] L. K. Tamm, J. Crane and V. Kiessling, Membrane fusion: a structural perspective on the interplay of lipids and proteins, *Current Opinion in Structural Biology*, (Elsevier) 13 (2003) 453-466.

- [35] S. A. Tatulian, P. Hinterdorfer, G. Baber and L. K. Tamm, Influenza hemagglutinin assumes a tilted conformation during membrane fusion as determined by attenuated total reflection FTIR spectroscopy, *EMBO J.* 14 (1995) 5514-5523.
- [36] N. K. Vaidya, H. Huang and S. Takagi, Modeling HA-protein mediated interaction between an influenza virus and a healthy cell: prefusion membrane deformation, *Math. Med. Biol.* 24 (2007) 251-270.
- [37] J. Zimmerberg, S. S. Vogel and L. V. Chernomordik, Mechanism of membrane fusion, *Ann. Rev. Biophys. Biomol. Struct.* 22 (1993) 433-466.

Appendix

The position of the membrane is as follows:

$$x(s) = \begin{cases} x_0 + \frac{\sin(Q_1 s)}{Q_1}, & 0 \leq s < a - r_1; \\ x_0 + \frac{\sin(Q_1(a-r_1))}{Q_1} + \frac{\sin(Q_2 s - P_2) - \sin(Q_2(a-r_1) - P_2)}{Q_2}, & a - r_1 \leq s < a; \\ x_0 + \frac{\sin(Q_1(a-r_1))}{Q_1} + \frac{\sin(Q_2 a - P_2) - \sin(Q_2(a-r_1) - P_2)}{Q_2} + \frac{\sin(Q_3 s - P_3) - \sin(Q_3 a - P_3)}{Q_3}, & a \leq s < b; \\ x_0 + \frac{\sin(Q_1(a-r_1))}{Q_1} + \frac{\sin(Q_2 a - P_2) - \sin(Q_2(a-r_1) - P_2)}{Q_2} + \frac{\sin(Q_3 b - P_3) - \sin(Q_3 a - P_3)}{Q_3} + \frac{\sin(Q_4 s + P_4) - \sin(Q_4 b + P_4)}{Q_4}, & b \leq s < b + r_2; \\ x_0 + \frac{\sin(Q_1(a-r_1))}{Q_1} + \frac{\sin(Q_2 a - P_2) - \sin(Q_2(a-r_1) - P_2)}{Q_2} + \frac{\sin(Q_3 b - P_3) - \sin(Q_3 a - P_3)}{Q_3} + \frac{\sin(Q_4(b+r_2) + P_4) - \sin(Q_4 b + P_4)}{Q_4} + \frac{\sin(Q_5 s - P_5) - \sin(Q_5(b+r_2) - P_5)}{Q_5}, & b + r_2 \leq s \leq L, \end{cases}$$

$$y(s) = \begin{cases} y_0 + \frac{1 - \cos(Q_1 s)}{Q_1}, & 0 \leq s < a - r_1; \\ y_0 + \frac{1 - \cos(Q_1(a - r_1))}{Q_1} + \frac{\cos(Q_2 s - P_2) - \cos(Q_2(a - r_1) - P_2)}{Q_2}, & a - r_1 \leq s < a; \\ y_0 + \frac{1 - \cos(Q_1(a - r_1))}{Q_1} + \frac{\cos(Q_2 a - P_2) - \cos(Q_2(a - r_1) - P_2)}{Q_2} + \frac{\cos(Q_3 a - P_3) - \cos(Q_3 s - P_3)}{Q_3}, & a \leq s < b; \\ y_0 + \frac{1 - \cos(Q_1(a - r_1))}{Q_1} + \frac{\cos(Q_2 a - P_2) - \cos(Q_2(a - r_1) - P_2)}{Q_2} + \frac{\cos(Q_3 a - P_3) - \cos(Q_3 b - P_3)}{Q_3} + \frac{\cos(Q_4 s + P_4) - \cos(Q_4 b + P_4)}{Q_4}, & b \leq s < b + r_2; \\ y_0 + \frac{1 - \cos(Q_1(a - r_1))}{Q_1} + \frac{\cos(Q_2 a - P_2) - \cos(Q_2(a - r_1) - P_2)}{Q_2} + \frac{\cos(Q_3 a - P_3) - \cos(Q_3 b - P_3)}{Q_3} + \frac{\cos(Q_4(b + r_2) + P_4) - \cos(Q_4 b + P_4)}{Q_4} + \frac{\cos(Q_5(b + r_2) - P_5) - \cos(Q_5 s - P_5)}{Q_5}, & b + r_2 \leq s \leq L. \end{cases}$$